4

Water–atmosphere parameterizations

4.1 Introduction

Pictures of the Earth from space often show a small blue and white ball on a black background. While we often think of the Earth as being green in color, in reality most of our planet's surface has a bluish color owing to the prevalence of the oceans. Oceans cover 70% of the Earth's surface, with an average depth of nearly 4 km, and as a major component in the global hydrological cycle liquid water is an essential resource for the survival of all animals and plants. It is perhaps not surprising to learn that to predict the Earth's climate, or to provide an accurate weather forecast, one must understand how the atmosphere and the ocean interact, and be able to represent these processes in numerical weather prediction models.

Air–sea interactions occur across a wide range of spatial and temporal scales. The ocean influences the atmosphere predominantly through variations in sea surface temperature (SST) and its effects on surface fluxes into the atmosphere, while the atmosphere influences the ocean predominantly through variations in the stress exerted upon the ocean surface by low-level winds. However, the interactions occurring on any given day are often much more complicated.

Surface fluxes of sensible and latent heat from the ocean surface to the atmosphere can play a significant role in the development and evolution of large-scale atmospheric disturbances such as extratropical cyclones, tropical cyclones, and polar lows. Bosart (1999) summarizes our present understanding of the importance of air–sea interaction to extratropical cyclones by stating that fluxes from the ocean surface can act to favorably precondition the atmosphere for cyclogenesis by enhancing the low-level baroclinicity. This is particularly true near warm ocean currents such as the Gulf Stream in the Atlantic Ocean and the Kuroshio Current in the Pacific Ocean, where

climatologies indicate that explosively deepening cyclones are most common (Sanders and Gyakum 1980). Bosart (1999) further suggests that the role of ocean surface fluxes in cyclogenesis is time, region, and life cycle dependent, with the fluxes most important early in the life cycle of a cyclone when environmental preconditioning occurs.

With regard to tropical cyclones, Anthes (1982, p. 49) remarks that one of the "remarkable relationships of tropical cyclone climatology is the existence of a threshold sea-surface temperature below which tropical cyclones do not form." This threshold temperature is 26.5 °C (Anthes 1982) and clearly suggests the importance of the oceans to these very intense cyclones. Indeed, Emanuel (1986) proposes an air–sea interaction instability mechanism in which tropical cyclones develop and are maintained by self-induced anomalous surface fluxes from the ocean, requiring only an initial finite-amplitude disturbance to begin the process. Hong *et al.* (2000) examine the interactions between Hurricane Opal (1995) and a circular region of warm water (called a warm core ring and associated with the so-called loop current) within the Gulf of Mexico. They show that the warm core ring assisted in the intensification of Opal, while the oceanic response to Opal resulted in a negative feedback that limited the intensification of the hurricane.

Sensible and latent heat fluxes from the ocean also are important to polar lows (Rasmussen 1985; Bresch *et al.* 1997) and small, quasi-tropical cyclones that form over the western Mediterranean in the fall (Homar *et al.* 2003). Polar lows are a special type of marine cyclogenesis event, where the low is not associated with a frontal boundary, is of relatively small horizontal scale (1000 km diameter or less) and shallow vertical extent, and forms near strong sea and air temperature gradients. They are most frequently observed over the North Atlantic and North Pacific Oceans. Thus, in areas where cyclones are observed over water, the fluxes of sensible and latent heat from the water surface can play a large role in the development and evolution of these systems.

However, even in regions and seasons where cyclones are infrequent, surface fluxes from the ocean play a large role in the structure of the overlying marine atmospheric boundary layer and in mesoscale structures within the boundary layer. Strong gradients in SST can help to produce atmospheric frontal zones (Holt and Raman 1992; Sublette and Young 1996), low-level jets (Doyle and Warner 1990), clouds (Carson 1950), and rain bands (Hobbs 1987; Holt and Raman 1992). Waters cooler than the overlying atmospheric boundary layer tend to stabilize the atmosphere, while waters warmer than the overlying atmospheric boundary layer tend to destabilize the boundary layer (Sweet *et al.* 1981). In coastal zones, the land–sea surface temperature contrast can lead to the development of sea and land breezes (Atkinson 1981).

On much longer timescales, the persistent and extensive warming of the eastern tropical Pacific Ocean called El Niño produces a global atmospheric response (Philander 1989). The El Niño Southern Oscillation (ENSO) is perhaps the best known example of air–sea interaction. Every 3 to 7 years, the typically cool waters of the eastern tropical Pacific warm by several degrees Celsius as the easterly trade winds weaken. This eastward extension of the warm ocean waters leads to an eastward shift in the region of tropical atmospheric deep convection and its associated upper-level divergence, shifting the source of Rossby wave train generation that can influence global circulation patterns (Tribbia 1991), especially during the winter months. The SST patterns in the tropical Atlantic Ocean also are known to influence seasonal precipitation amounts in sub-Saharan Africa (Lamb 1978a, b; Lamb and Peppler 1992).

The oceans also play the key role in defining the amount of water vapor in the atmosphere. Cold polar air masses are significantly modified as they move over the warmer waters of the Gulf of Mexico (Henry and Thompson 1976; Liu *et al.* 1992). The warming and moistening of the air mass over the gulf waters leads to a doubling of the boundary layer depth as well as a dramatic moistening of the boundary layer in less than a day. These studies illustrate how quickly oceans can modify air masses that originate over land. On seasonal timescales, Hastenrath (1966) and Rasmussen (1967) both show that there is a strong moisture flux from the Caribbean Sea over the Gulf of Mexico and into North America during the summertime. These results should not be a surprise, since water vapor is released mainly in the subtropical oceans and is transported both equatorward and poleward to supply the observed precipitation regions in the Tropics and the midlatitudes (Peixoto and Oort 1992). In the midlatitudes, most of the poleward transport of water vapor occurs in atmospheric rivers (Zhu and Newell 1998) or moisture conveyor belts (Bao *et al.* 2006), filaments of air with high water vapor content associated with extratropical cyclones. Further underscoring the importance of the oceans to the hydrological cycle, Peixoto and Kettani (1973) indicate that evaporation from the oceans is six times larger than evaporation from the land masses.

While these studies indicate the importance of the ocean to the atmosphere, the reverse is also true. As mentioned earlier, ENSO events begin with the weakening of the easterly trade winds in the eastern Pacific Ocean (Tribbia 1991). This weakening allows the warmer waters in the western Pacific to flow eastward. Also on these longer timescales, water vapor that is transported poleward precipitates either directly into the oceans or over land, where a portion of the precipitation flows into rivers and is eventually discharged back into the oceans, influencing the temperature and salinity of the ocean waters.

On shorter timescales, the atmosphere influences the ocean due to both the forcing of local surface winds and heat transfer. The presence of cold continental air and strong winds over the Gulf Stream, in association with the passage of an extratropical cyclone, lead to enhanced mixing of the ocean mixed layer. In addition, the heat transferred by the water to the cold low-level air leads to a decrease in Gulf Stream water temperature (Bane and Osgood 1989; Xue *et al.* 1995) as the heat transfer to the atmosphere is balanced by the cooling of the upper water column of the ocean (Xue *et al.* 1995, 2000; Xue and Bane 1997). Over shallow shelf waters, extended cold air outbreaks can lead to decreases in water temperature of 5 °C or more over a 10 day period (Nowlin and Parker 1974). This decrease in water temperature becomes smaller as the shelf water depth increases. The stronger atmospheric surface winds and the cooling of the ocean waters also can lead to enhanced mixing in the ocean mixed layer and a deepening of this layer (Bane and Osgood 1989; Adamec and Elsberry 1985), which produces a small negative feedback on the surface fluxes to the atmosphere.

Tropical cyclones also influence ocean temperatures, with lower temperatures observed following the passage of tropical cyclones over a region (Fisher 1958; Jordan 1964; Leipper 1967). Sea surface temperature decreases of 5 °C are not unusual, and may be produced by upwelling of cooler ocean water, wind-induced mixing of ocean water, heat lost to the atmosphere, and horizontal advection of cooler water.

In coastal zones, strong surface winds also can produce upwelling of ocean water. Under certain atmospheric conditions, gaps in the local coastal terrain can produce very strong offshore winds (gusts in excess of $60\,m\,s^{-1}$), leading to enhanced vertical mixing of the ocean waters and upwelling along the coast (Schultz *et al.* 1997). Sea surface temperature decreases of 8 °C have been observed in a few hours in association with these gap winds in the Gulf of Tehuantepec off the southern coast of Mexico (Stumpf 1975; Schultz *et al.* 1997).

In addition to the mixing and cooling of ocean waters, the atmospheric surface winds also can influence ocean currents. In a cold air outbreak over the Gulf Stream, the upper ocean responds strongly to the local wind field producing a $20\,cm\,s^{-1}$ flow in a coupled atmosphere–ocean model (Xue *et al.* 2000). In response to the even stronger winds from a tropical cyclone over the Gulf of Mexico, Brooks (1983) shows that a southward current surge reaching $91\,cm\,s^{-1}$ is observed at 200 m depth coincident with a 4 °C temperature increase and a 3% salinity increase. A wake oscillation forms after the passage of the cyclone eye having a near-inertial period and currents approaching $50\,cm\,s^{-1}$. This wake decays with a timescale of ~5 days.

Owing to the importance of the oceans to the Earth's climate, the latest generation of global climate models are coupled ocean–atmosphere models. Models are developed separately for both the oceans and for the atmosphere and linked through the interactions that occur between the ocean and the atmosphere. For operational numerical weather prediction models, the ocean often has a prescribed SST, based upon observations, that is held constant throughout the forecast period or relaxed towards climatology. Regardless of the approach used, the parameterizations of the air–sea interactions are very important to the resulting forecasts or simulations.

4.2 Observing sea surface temperature

The most important variable needed in meteorological models over the oceans is the SST. Thankfully, satellite data can be used to observe SSTs routinely, since *in situ* observations over the oceans are sparse. The approaches used most commonly are similar to that of Reynolds and Smith (1994), who develop an optimum interpolation approach to produce weekly and daily 1.0° analyses of SST from both satellite and *in situ* data. Presently, analyses of SST with horizontal grid spacings of 0.5° are common (Thiebaux *et al.* 2003) and grid spacings as small as 14 km are available over some regions. Seas and large lakes, such as the Mediterranean, Red, Black, and Caspian Seas and the Great Lakes, also are included in these analyses. Smaller lakes are not included.

The satellite observations are from the National Oceanic and Atmospheric Administration's Advanced Very High Resolution Radiometer (AVHRR) on board polar-orbiting satellites. Combined, these satellites pass over any given location on the Earth several times a day. Two infrared channels within the atmospheric window are used to produce a multichannel SST retrieval with a horizontal resolution of approximately 8 km (McClain *et al.* 1985; Walton 1988). Different algorithms are used for daytime and nighttime satellite observations. While these satellite data have very good horizontal resolution and global coverage (Fig. 4.1), they are limited to sampling in cloud-free areas, generally provide sparse data near ice edges in the poles, and can be biased by the presence of atmospheric aerosols.

The *in situ* data are from ships and buoys. The distribution of these observations depends upon shipping traffic and is most dense in the northern hemisphere and least dense in the southern hemisphere (Fig. 4.2). A number of the buoy locations have been selected to improve data coverage in regions where shipping traffic is minimal (Fig. 4.3). These *in situ* data also

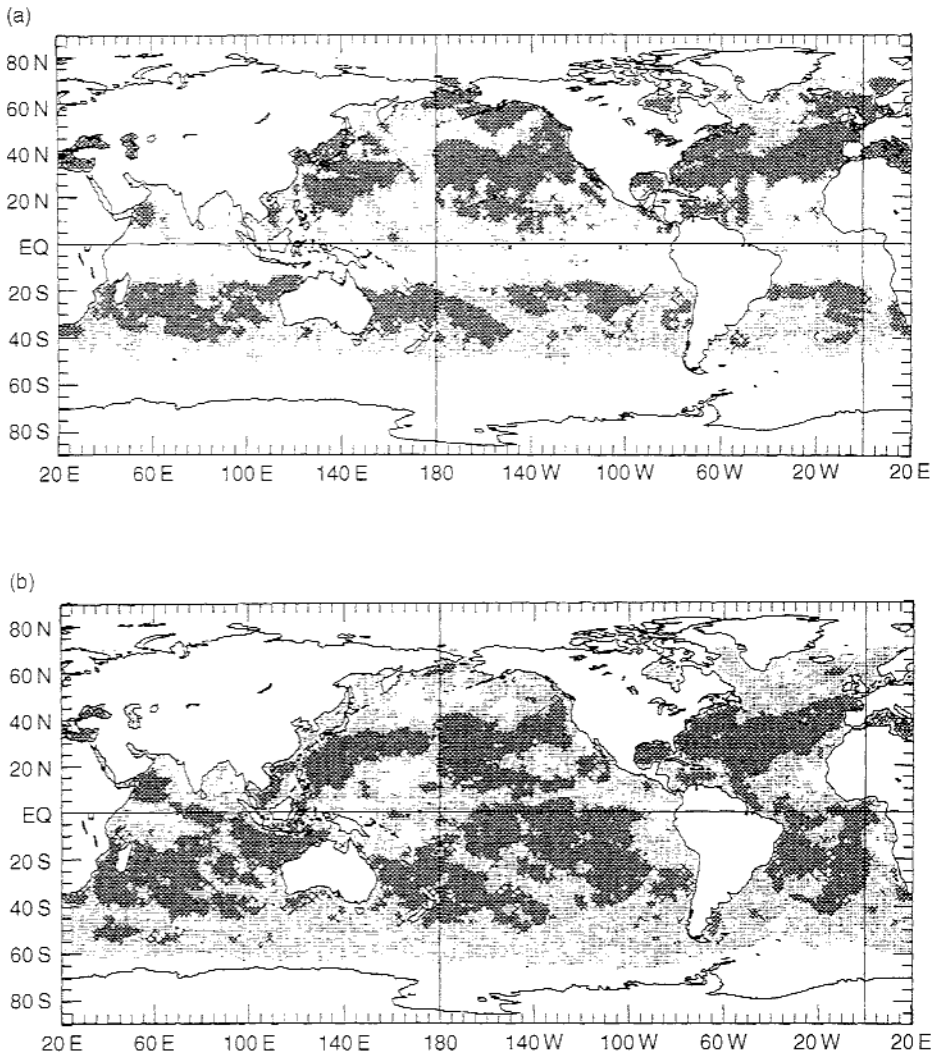

Figure 4.1. The distribution of AVHRR daytime (top) and nighttime (bottom) retrievals within 1° latitude–longitude grid cells for the week of 4–10 August 1991. A dot indicates that one to nine observations are present within the grid cell, while an X indicates ten or more observations. From Reynolds and Smith (1994).

provide sparse coverage near the ice edge, requiring additional information on sea ice based upon satellite observations of brightness temperature (e.g., Cavalieri *et al.* 1991) from the special sensor microwave imager (SSM/I) on board the defense meteorological satellite program (DMSP) polar-orbiting satellites.

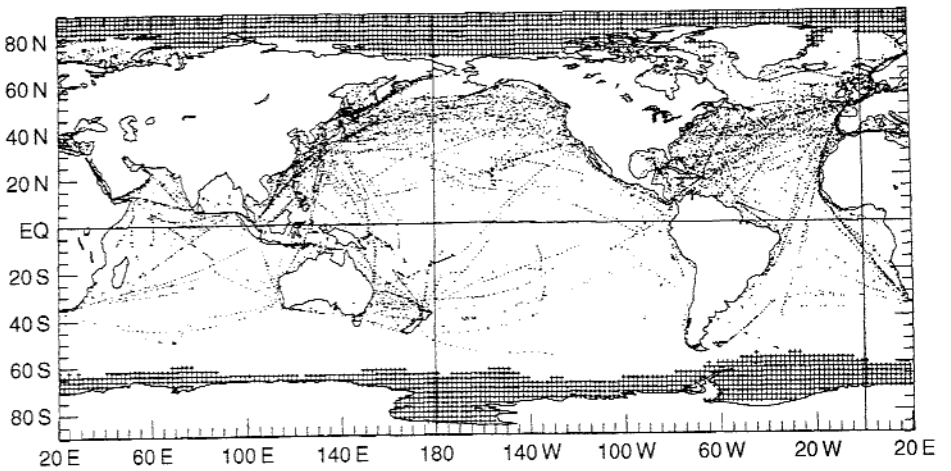

Figure 4.2. Distribution of ship observations available during the week of 4–10 August 1991. Gridded sea ice observations are denoted by a plus sign. From Reynolds and Smith (1994).

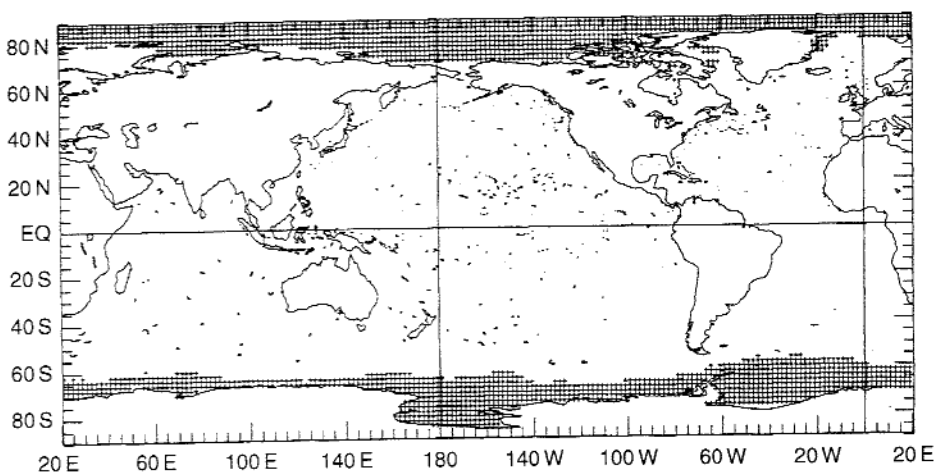

Figure 4.3. The distribution of buoy observations during August 1991. Gridded sea ice observations indicated by a plus sign. From Reynolds and Smith (1994).

Once the satellite and *in situ* data are processed and quality controlled, they generally are combined into a single analysis of SST once every day following the optimum interpolation method of Reynolds and Smith (1994). This approach includes the previous SST analysis as a first guess, incorporates seven days worth of data, and uses a Poisson technique to correct for any biases in the satellite observations as determined from comparisons with the *in situ* SST observations from ships and buoys. The importance of the bias

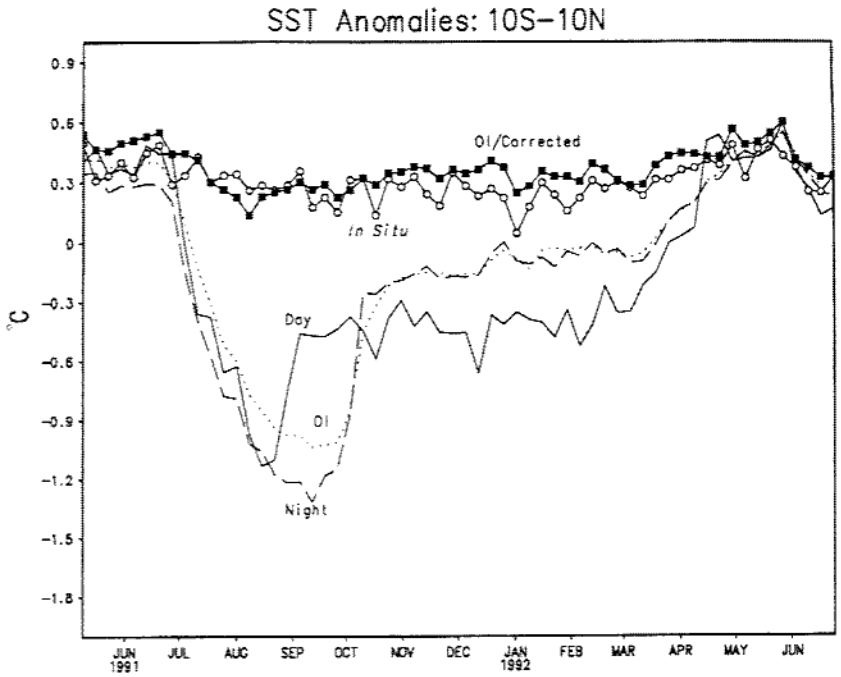

Figure 4.4. Zonally averaged anomalies of SST for the latitude band from 10° S to 10° N from May 1991 through July 1992. The curves show the *in situ* (open circles), daytime (solid) and nighttime (dashed) satellite retrievals, the optimum interpolation without satellite data bias correction (dotted), and the optimum interpolation with satellite data bias correction (solid squares) anomaly values. Mt. Pinatubo in the Philippines (latitude 15° N) erupted on 15 June 1991 and affected the satellite SST retrievals through April 1992. From Reynolds and Smith (1994).

correction to the satellite data is clearly seen when aerosols are injected into the atmosphere from volcanic eruptions (Fig. 4.4). The end result of the optimum interpolation is a global SST field that contains a fair amount of detail (Fig. 4.5). Other recent approaches use the AVHRR satellite data, but also must blend the satellite data with *in situ* observations (Thiebaux *et al.* 2003), or microwave data (Chelton and Wentz 2005). Now that the ocean SST is defined, we can turn our attention to how the surface fluxes of sensible and latent heat are calculated.

4.3 Sensible heat flux

The main differences between flow over land as discussed in Chapter 2 and flow over the ocean are the undulating, wavy nature of the ocean surface and the large heat capacity of the ocean. This means that the surface roughness

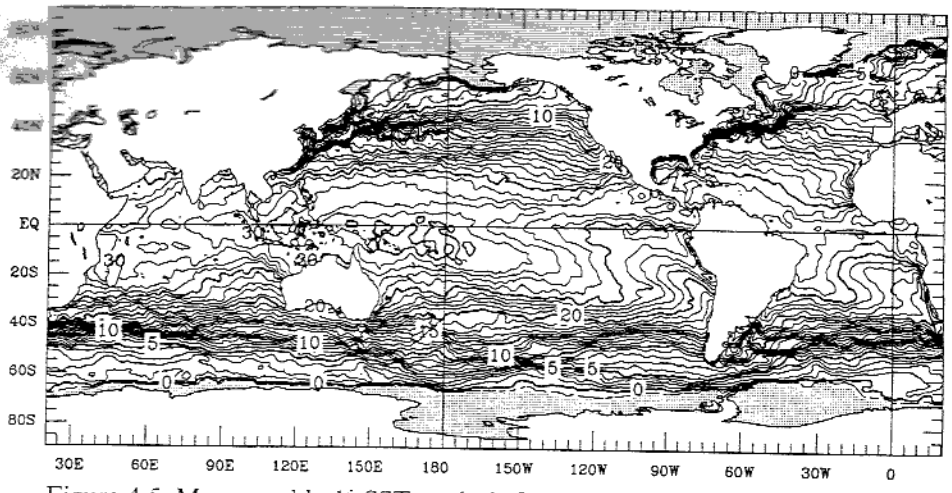

Figure 4.5. Mean weekly 1° SST analysis from 13–19 January 1991. Isolines every 1 °C, with heavy isolines every 5 °C starting with 1 °C. The −1 °C isoline is dashed, and SSTs below −1.78 °C are shaded and generally indicate regions of sea ice. The freezing point for sea water in the polar regions is near −1.8 °C. From Reynolds and Smith (1994).

length depends upon the state of the ocean surface, and that the values of SST can be held constant for relatively short numerical weather forecasts. In general, SSTs are held constant for short-range (0–4 day) and medium-range (5–14 day) weather forecasts. For seasonal and climate predictions, a coupled ocean–atmosphere modeling system is needed.

The equation for sensible heat flux is exactly the same basic form as found in Chapter 2, namely

$$Q_H = \frac{\rho c_p [T_{SST} - T(z)]}{r_H}, \tag{4.1}$$

where T_{SST} is the sea surface temperature (K), r_H is the resistance (s m^{-1}), $T(z)$ is the temperature (K) at height z, ρ is the atmospheric density (kg m^{-3}), and c_p is the specific heat at constant pressure (J K^{-1} kg^{-1}). The resistance is again defined as

$$r_H = \frac{1}{k u_*}\left[\ln\left(\frac{z}{z_0}\right) - \psi_h\left(\frac{z}{L}\right)\right] + \frac{1}{k u_*}\ln\left(\frac{z_0}{z_{0h}}\right), \tag{4.2}$$

where z_0 is the roughness length (m), z_{0h} is the roughness length for sensible heat flux, u_* is the friction velocity, k is von Karman's constant (~0.4), z is the depth over which the resistance is calculated (m), ψ_h is the stability function for non-neutral conditions, and L is the Monin–Obukhov length (m).

As shown in Fairall *et al.* (2003), the main differences from the calculation of (4.1) over the ocean as compared to over land are that the roughness lengths are different and depend upon the ocean state and that the calculation of u_* incorporates another factor for conditions of no wind. If one defines the mean wind speed $S(z)$ so that it incorporates a gustiness factor u_g, in which

$$u_g = \beta \left[\frac{g z_i}{T} (\overline{w'\theta'_v}) \right]^{1/3} = \beta w^*, \tag{4.3}$$

where g is the acceleration due to gravity ($\mathrm{m\,s^{-2}}$), T is temperature (K), z_i is the atmospheric boundary layer depth, $\overline{w'\theta'_v}$ is the surface buoyancy flux, β is a scaling parameter (= 1.25), and w^* is the free convection scaling velocity (Stull 1988), then

$$S(z) = \left(u^2 + v^2 + u_g^2 \right)^{1/2}, \tag{4.4}$$

where u and v are the horizontal wind components at height z. Using these definitions, one can finally define a slightly modified u_* as

$$u_* = \frac{S(z)k}{[\ln(z/z_0) - \psi_m(z/L)]}, \tag{4.5}$$

where $S(z)$ is replaced by $u(z)$ in the original definition when $u_g = 0$.

The only other needed parameters are the roughness lengths z_0 and z_{0h}. The definitions of roughness length over the oceans often refer back to the study of Charnock (1955), who defined a relation for rough flow over the sea. This relation is given by

$$z_0 = \alpha_c u_*^2 / g, \tag{4.6}$$

where α_c is referred to as Charnock's constant. Typically, α_c has a value near 0.011 with values ranging from 0.005 to 0.025 (Fairall *et al.* 2003). Smith (1988) adds a smooth flow limit, yielding

$$z_0 = \alpha_c u_*^2 / g + 0.11 \nu / u_*, \tag{4.7}$$

where ν is the kinematic viscosity ($\mathrm{m^2\,s^{-1}}$). In some parameterizations, α_c is a constant (Zeng *et al.* 1998), while in others it increases as a function of wind speed (Fairall *et al.* 2003).

Many of the parameterizations have different formulations for the stability function profiles ψ_m and ψ_h as is also seen in the parameterizations over land surfaces. It is not certain if the Monin–Obukhov similarity theory used in developing the stability function profiles over land is valid over an undulating

water surface. This yields a fair amount of uncertainty in the use and definition of the stability functions ψ_m and ψ_h. In particular, Fairall *et al.* (2003) recommend using a power-law relationship for the stability function calculation when $z/L < -1$ during convective conditions.

Bourassa *et al.* (1999, 2001), Taylor and Yelland (2001), and Oost *et al.* (2002) relate the values of z_0 to aspects of the sea state, such as swell, gravity waves, and capillary waves. Capillary waves are the shortest waves (generally less than a few centimeters in wavelength) and are commonly called ripples. The primary restoring force for capillary waves is surface tension. While capillary waves can be neglected for high wind speeds, Bourassa *et al.* (2001) argue that the sum of the effects of all capillary waves to surface roughness cannot be ignored for light wind speeds because there are so many capillary waves compared to other waves in the ocean. Gravity waves are the dominant wave features we see visually on the ocean surface. Swell refers to gravity waves that are not growing or sustained by the surface winds, one example of which is waves when the local winds are calm.

The basic idea behind these parameterizations is that the roughness length is determined principally by the steepest waves. Thus, Taylor and Yelland (2001) suggest

$$z_0 = 1200 h_s \left(\frac{h_s}{L_p}\right)^{4.5}, \tag{4.8}$$

where h_s is the significant wave height (m) and L_p is the wavelength (m) associated with the peak of the wave frequency–size spectrum with its associated dominant wave period T_p. The wavelength L_p can be determined from T_p using the standard deep-water gravity wave relationship

$$L_p = \frac{g T_p^2}{2\pi}, \tag{4.9}$$

while the value of h_s is determined empirically from formulas for a fully developed sea in which

$$h_s = 0.0248[u_n(10\,\mathrm{m})]^2, \tag{4.10}$$

where $u_n(10\,\mathrm{m})$ is the wind speed at 10 m under neutral conditions. Finally, the value of T_p is also determined empirically using

$$T_p = 0.729 u_n(10\,\mathrm{m}). \tag{4.11}$$

In a similar approach, Oost *et al.* (2002) relate the phase speed C_p of the dominant wave to the friction velocity u_* in order to obtain a measure of wave age, which is then related to the roughness length. In their study using data

Table 4.1. *Values for the coefficients a_h and b_h for specifying z_{0h} and a_v and b_v for specifying z_{0v} as a function of the roughness Reynolds number R_r. Values from Liu* et al. *(1979).*

R_r	a_h	b_h	a_v	b_v
0–0.11	0.177	0	0.292	0
0.11–0.825	1.376	0.929	1.808	0.826
0.925–3.0	1.026	−0.599	1.393	−0.528
3.0–10.0	1.625	−1.018	1.956	−0.870
10.0–30.0	4.661	−1.475	4.994	−1.297
30.0–100.0	34.904	−2.067	30.790	−1.845

from several field campaigns in the North Sea, they find that Charnock's parameter is related to wave age by

$$\alpha_c = 50\left(\frac{C_p}{u_*}\right)^{-2.5}. \tag{4.12}$$

Finally, the determination of the roughness length for heat, z_{0h}, also requires a different relationship than over land. Liu *et al.* (1979) suggest that

$$z_{0h} = \frac{\nu}{u_*} f_h(R_r) = \frac{\nu}{u_*} a_h R_r^{b_h}, \tag{4.13}$$

where R_r is the roughness Reynolds number ($R_r = u_* z_0 / \nu$), and the values of a_h and b_h depend upon the value of R_r and range from 0.17 to 35 for a_h and −2.1 to 0.93 for b_h. Table 4.1 is taken from Liu *et al.* (1979) and specifies the details on the values for a_h and b_h as a function of R_r.

A slightly different relationship is suggested by Brutsaert (1982), in which

$$z_{0h} = \begin{cases} ae^{-bu_*^{1/4}}, & \text{for rough surfaces,} \\ \dfrac{d\nu}{u_*}, & \text{for smooth surfaces,} \end{cases} \tag{4.14}$$

where $a = 0.169$, $b = 1.53$, and $d = 0.624$. Rough surfaces occur when $R_r > 0.13$. This approach is used by Zeng *et al.* (1998). Others relate z_{0h} to z_0 directly using the values of u_* (Makin and Mastenbroek 1996) or R_r (Garratt 1992; Zilitinkevich *et al.* 2001).

Both sensible and latent heat fluxes are modified when sea spray is present. Sea spray typically is observed for wind speeds in excess of $15\,\mathrm{m\,s^{-1}}$, may be present for wind speeds as low as $7\,\mathrm{m\,s^{-1}}$, and is produced by wind gusts, bursting bubbles, and breaking waves (Kraus and Businger 1994; Andreas *et al.* 1995) as illustrated in Fig. 4.6. The presence of sea spray produces an

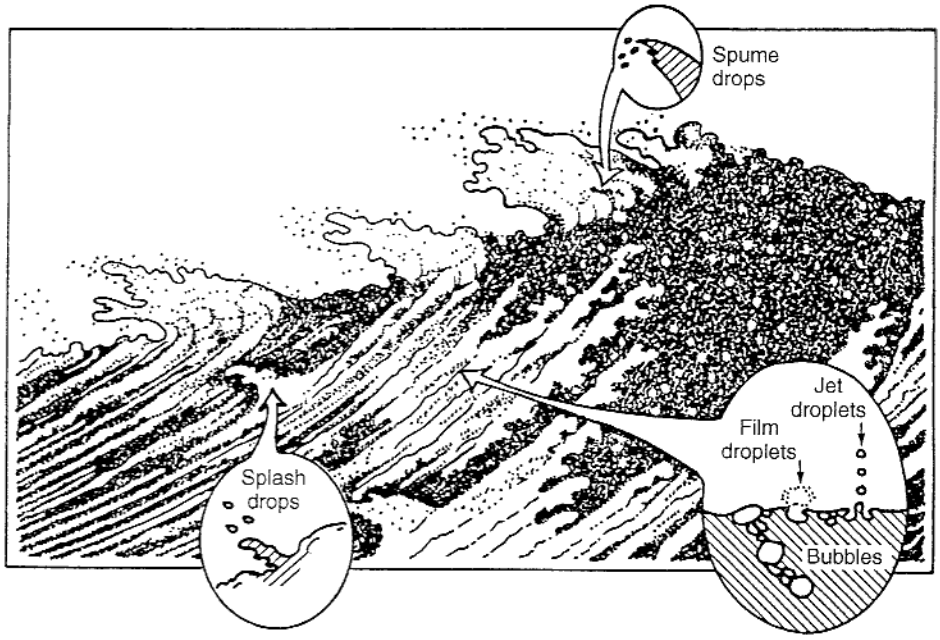

Figure 4.6. Illustration of how sea spray droplets originate. Splash droplets occur when wave crests spill, film and jet droplets occur where bubbles rise and burst, and spume droplets occur at the crests of steep waves and are torn directly from the crests by the wind. The general form of the illustration is based on one by Hokusai (*c.* 1833). From Andreas *et al.* (1995).

atmospheric layer in which the droplets are evaporating and their temperature comes into equilibrium with the environment, thereby altering the surface sensible and latent heat fluxes. Sea spray droplets initially accelerate horizontally as they are injected into the atmosphere, quickly reaching the low-level wind speed and producing a net drag on the airflow.

Relatively simple scaling relationships to parameterize the effects of the sea spray are documented in Andreas (1992), Andreas *et al.* (1995), Fairall *et al.* (1994), and Andreas and DeCosmo (1999). More recently, Andreas and Emanuel (2001) explore the effects of re-entrant spray in which the larger spray droplets fall back into the ocean prior to their complete evaporation. They show that the timescale for the spray droplet to reach its equilibrium temperature is very short, of the order of 1 s, and requires very little evaporation (Fig. 4.7). In contrast, the timescale for the spray droplet to reach its equilibrium radius is much longer, of the order of 100 s, suggesting that the droplet can fall back into the ocean prior to reaching its equilibrium radius. The net effect of this re-entrant spray is that the droplets give up heat to the atmosphere as they cool, yet many droplets fall back into the sea before extracting from the air the heat needed to evaporate. This yields a net sea-to-air

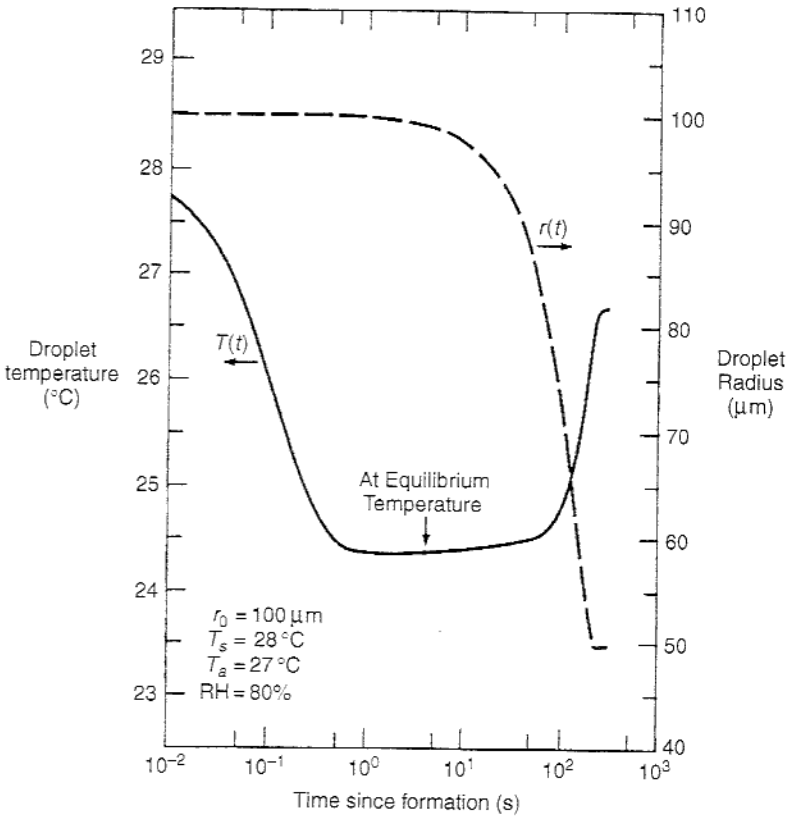

Figure 4.7. The temperature (T) and radius (r) of a sea spray droplet (100 μm initial radius and initial salinity of 34 practical salinity units) versus time (s) that is ejected from a 28 °C ocean surface into air of 27 °C with 80% relative humidity and a barometric pressure of 1000 hPa. Note that the droplet equilibrium temperature is much less than air temperature and is reached within 1 s of droplet ejection, whereas it takes over 100 s for the droplet radius to reach equilibrium. From Andreas and Emanuel (2001).

enthalpy flux that may be very important to tropical cyclone intensification as wind speeds increase to near hurricane force (Andreas and Emanuel 2001). New measuring technologies are needed to measure spray in high wind conditions to validate these spray parameterizations over the entire range of atmospheric environments (Andreas *et al.* 1995).

4.4 Latent heat flux

As with the sensible heat flux, the expression for the latent heat flux from a water surface takes on exactly the same formulation as for over land, but with a few modifications in the details. The latent heat flux can be defined as

$$Q_E = \frac{\rho L_v (q_{S\_SST} - q(z))}{r_{V(0,z)}}, \tag{4.15}$$

where L_v is the latent heat of vaporization ($J\,kg^{-1}$), q_{S_SST} is the saturation specific humidity at the SST, $q(z)$ is the specific humidity at height z, and r_V is the resistance to latent heat flux ($s\,m^{-1}$). It is important to note that the saturation specific humidity at the SST is computed from the SST and the vapor pressure of sea water, which equals 0.98 times the vapor pressure of pure water (Kraus and Businger 1994). As in the discussion of sensible heat flux over water, the stability function profiles described using Monin–Obukhov similarity theory may not apply well to an undulating ocean surface and the effects of sea spray should be considered for wind speeds above $15\,m\,s^{-1}$.

The resistance is defined exactly as in Chapter 2, using

$$r_{V(0,z)} = \frac{1}{k u_*}\left[\ln\left(\frac{z}{z_0}\right) - \psi_h\left(\frac{z}{L}\right)\right] + \frac{1}{k u_*}\ln\left(\frac{z_0}{z_{0v}}\right), \tag{4.16}$$

where z_{0v} is the roughness length for latent heat flux. A number of options for the calculation of z_0 are described above for the calculation of sensible heat flux. However, the equations for calculating z_{0v} can be quite different from those of z_{0h}.

Liu *et al.* (1979) suggest a similar form for the z_{0h} and z_{0v} relationships, with

$$z_{0v} = \frac{\nu}{u_*} f_v(R_r) = \frac{\nu}{u_*} a_v R_r^{b_v}, \tag{4.17}$$

where the parameters a_v and b_v depend upon the value of R_r. The parameter values in Table 4.1 are from Liu *et al.* (1979) and show that a_v varies from 0.29 to 30.79 while b_v varies from -1.85 to 0.83.

Fairall *et al.* (2003) suggest the following empirical fit for z_{0v} that describes well the observed fluxes calculated during the Coupled Ocean–Atmosphere Experiment (COARE) and Humidity Exchange Over the Sea (HEXOS), such that

$$z_{0v} = \min(1.1 \times 10^{-4}, 5.5 \times 10^{-5} R_r^{-0.6}). \tag{4.18}$$

Garratt (1992) relates z_{0v} to both z_0 and R_r, yielding

$$z_{0v} = z_0 \exp(2 - 2.28 R_r^{1/4}). \tag{4.19}$$

Other approaches again are found in Makin and Mastenbroek (1996) and Zilitinkevich *et al.* (2001). The effects of sea spray may also influence the latent heat flux and so must be taken into account for higher wind speeds (Andreas 1992, 1998; Fairall *et al.* 1994; Andreas *et al.* 1995; Andreas and DeCosmo 1999).

4.5 Coupled ocean–atmosphere models

For seasonal and climate simulations or predictions, and for studies of hurricanes, coupled ocean–atmosphere models often are used. In these coupled modeling systems there are actually up to three models in use: an atmospheric model, an ocean model, and a wave model (see Bao *et al.* 2000; Powers and Stoelinga 2000). However, owing to computational costs, timescales of interest, and the intended application, many systems today couple two of these models, either an ocean–atmosphere coupled modeling system (e.g., Frey *et al.* 1997; Hodur 1997; Ineson and Davey 1997; Schneider *et al.* 1997; Stockdale *et al.* 1998; Gregory *et al.* 2000; Kanamitsu *et al.* 2002; Kiehl and Gent 2004) or a wave–atmosphere coupled modeling system (e.g., Weber *et al.* 1993; Doyle 1995, 2002; Gregory *et al.* 2000). The coupling takes place at the air–sea interface. For example, when all three models are used, the atmospheric model provides the surface stress to the wave model, which uses this information to derive the two-dimensional wave energy spectrum. The wave model provides the wave-induced roughness length to the atmospheric model for use in calculating the surface fluxes, which also requires the SST provided by the ocean model. The wave-induced stress from the wave model along with the surface fluxes and radiation from the atmospheric model are used by the ocean model to derive the SST.

While the synoptic observational data generally are sufficient to start an atmospheric model, observations over the oceans are sparse below the surface. This situation leads to the ocean model being run for months or years prior to the start time of any forecast or simulation in order to develop a representative three-dimensional ocean state. During this assimilation period, the ocean model is forced by surface wind stresses provided by global analyses or an atmospheric model, observed sea surface height anomalies derived from satellite data, and the observed SSTs (e.g., Bao *et al.* 2000). The wave models generally do not need to be initialized prior to the start of the coupled model simulation unless wave characteristics during the first day or so are important.

4.6 Discussion

Observing the oceans is very difficult. Radiation does not penetrate very far into the oceans, perhaps a few tens of meters, and so observations of any quantities not near the surface must be made from direct *in situ* measurements. This requires the use of ships or buoys, the cost of which can quickly become very expensive. While research observations have been sufficient to describe the basic large-scale ocean circulation and to provide an understanding of the

mechanisms for the major ocean currents, we have much less understanding of mixing and friction (Sarachik 2003).

In addition, observing sensible and latent heat fluxes over the ocean also is expensive and difficult, especially in high wind conditions associated with significant atmospheric phenomena, such as hurricanes and rapidly developing cyclones. This makes it very difficult to determine the impact of sea spray on the air–sea momentum and the sensible and latent heat fluxes. Thus, many parameterizations are developed using data within a limited range of conditions and are then extrapolated to the entire range visited by the atmosphere. For example, Bao *et al.* (2000) compare several roughness length schemes for surface sensible and latent heat flux over the oceans. All of these schemes apply to observed wind speeds of 20 m s^{-1} or less, but are extrapolated in models to much higher wind speeds. When evaluated in an idealized simulation of Hurricane Opal, the different roughness length schemes produce a large sensitivity in the intensity of the simulated hurricane (Fig. 4.8). Curiously, the use of one particular roughness length scheme results in no intensification at all, while other schemes result in differences in the minimum sea-level pressure of 17 hPa. This study illustrates both the large disparity in the formulas for surface roughness lengths and their very different behaviors when used within a numerical weather prediction model.

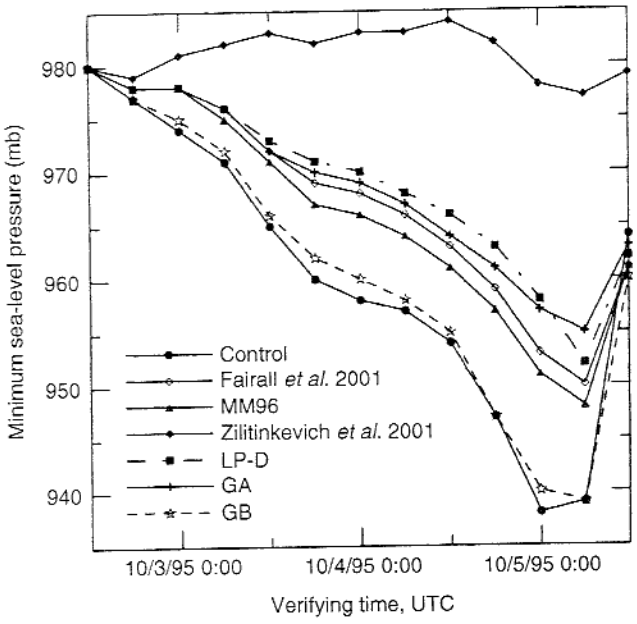

Figure 4.8. Minimum sea-level pressure of simulated hurricanes that use different roughness length schemes as compared with a control run. From Bao *et al.* (2000).

It also may be important to include the effects of sea ice in numerical weather prediction models. Sea ice is not uniform and incorporates many leads, or fractures between ice floes (ice sheets) sufficiently wide to be navigated by a ship and several kilometers in length. Leads are not very common during the winter season, but can be very prevalent during summer. While some leads are covered with a thin layer of ice, others are not. This can produce direct contact between the atmosphere and the ocean surface within widespread regions of sea ice. Several parameterizations of sea ice have been developed (Maykut and Untersteiner 1971; Ebert and Curry 1993; Hunke and Dukowicz 1997; Bitz and Lipscomb 1999) and are used in numerical models, especially for climate simulations. Finally, it is important to account for the air–sea gas transfer of CO_2 in climate simulations (Csanady 2001) as the oceans contain 56 times as much carbon as the atmosphere and dissolve roughly one-third of the CO_2 released by fossil fuels each year (Schlesinger 1997).

4.7 Questions

1. Go onto the world-wide web and search for a site that provides daily or weekly global SST analyses or regional SST analyses appropriate for your location and available over at least a 1 year period. Explore these data for a 1 year period and describe the SST evolution nearest to where you live. What is the typical range of SST values? Are there any features or structures that you can describe (e.g., currents, anomalies such as warm rings)? How do you think the oceans influence the weather where you live?
2. Using the sensible heat flux equation (4.1), examine the sensitivity to roughness lengths z_0 and z_{0h}. First, assume $\rho = 1.0\,\mathrm{kg\,m^{-3}}$, $T_{SST} = 303\,\mathrm{K}$, $T\,(10\,\mathrm{m}) = 300\,\mathrm{K}$, $L = -50\,\mathrm{m}$, $w* = 1.0\,\mathrm{m\,s^{-1}}$, the 10 m wind speed is $10\,\mathrm{m\,s^{-1}}$, $u_* = 0.8\,\mathrm{m\,s^{-1}}$, and viscosity $\nu = 1.46 \times 10^{-5}\,\mathrm{m^2\,s^{-1}}$. Determine z_0 using (4.7) and then z_{0h} from (4.13) and (4.14). Calculate Q_H using both values of z_{0h}. How sensitive are the results to the formulas used?
3. Using the results from Question 2, now calculate z_0 using (4.8) and assume that the neutral wind speed is equal to the assumed 10 m wind speed given. Recalculate the values of z_{0h} using (4.13) and (4.14) and again determine the values for Q_H. How sensitive is the value of Q_H to the values of z_{0h} and to the values of z_0?
4. We know that SST varies slowly in comparison to changes in the atmospheric surface layer, even over the tropical oceans far away from land. What processes could produce variability in the atmospheric surface layer over the oceans?